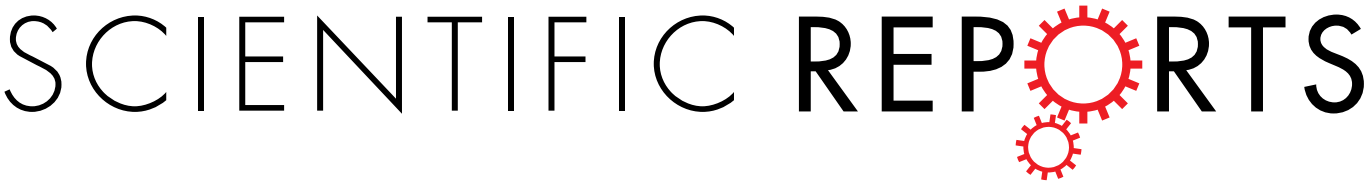

OPEN

Roles of vacuum tunnelling and contact mechanics in single-molecule thermopower

Received: 19 August 2016
Accepted: 06 February 2017
Published: 10 March 2017

Makusu Tsutsui, Kazumichi Yokota, Takanori Morikawa & Masateru Taniguchi

Molecular junction is a chemically-defined nanostructure whose discrete electronic states are expected to render enhanced thermoelectric figure of merit suitable for energy-harvesting applications. Here, we report on geometrical dependence of thermoelectricity in metal-molecule-metal structures. We performed simultaneous measurements of the electrical conductance and thermovoltage of aromatic molecules having different anchoring groups at room temperature in vacuum. We elucidated the mutual contributions of vacuum tunnelling on thermoelectricity in the short molecular bridges. We also found stretching-induced thermoelectric voltage enhancement in thiol-linked single-molecule bridges along with absence of the pulling effects in diamine counterparts, thereby suggested that the electromechanical effect would be a rather universal phenomenon in Au-S anchored molecular junctions that undergo substantial metal-molecule contact elongation upon stretching. The present results provide a novel concept for molecular design to achieve high thermopower with single-molecule junctions.

Thermoelectricity is a phenomenon wherein a temperature difference in a material induces energy flow via electrical charge diffusion from hot to cold side thereby providing a simple and environmentally-friendly way of converting heat into electricity in single step without any need of moving mechanical components equipped in many of today's thermal power generation systems[1]. Wide applications of this ideal convertor require compounds with high thermoelectric figure of merits[2–5]. Recently, there has been growing interest in exploring quantum confinement effects in low-dimensional structures for better thermoelectrics[6–11]. Alike the nanomaterials investigated to date, such as superlattices[12], nanotube/nanowires[13], and quantum dots[14], a single-molecule interconnected to metallic electrodes is a quantum system having discrete electronic states that promise giant thermopower by chemically-engineering the electronic structures through optimizing the molecular architectures[15–18]. Much progress has been accomplished in understanding and controlling the single-molecule thermoelectric transport properties, such as length dependence[19–21], intermolecular interactions[22], and gate control[23], owing to the advance in experimental techniques to address the electron and heat transport in molecular bridges[17]. In sharp contrast, the roles of electrode-molecule contacts on the thermoelectric properties have remained almost unexplored[24,25] albeit the theoretically predicted impact on the electronic structures[26–30], due mostly to the technical difficulty to evaluate the geometrical dependence of thermoelectricity in molecular junctions that requires a reliable method to form and hold a molecular bridge for long-enough time to measure their thermoelectric properties and meanwhile controllably deform the configurations at an atomistic level. In the present study, therefore, we report molecular junction diagnosis by thermoelectric analysis for characterizing the anchor dependence to geometrical sensitivity of single-molecule thermopower.

Results

Conductance and thermovoltage traces. We studied benzene molecules possessing amine and thiol groups at the *para* positions: 1,4-benzenedithiol (BDT), 1,4-benzenediamine (BDA), and 4-aminobenzenethiol (ABT) (Fig. 1a). Microheater-embedded lithographically-defined mechanically-controllable break junctions (MCBJs)[25] were employed to carry out simultaneous measurements of the conductance G and the thermovoltage ΔV_j of metal-molecule-metal junctions under stretching at a rate of 0.5 pm/s through a piezo-voltage (V_{piezo}) control with a temperature gradient imposed through Joule heat generated at the Pt coil with the applied voltage V_h at room temperature in vacuum (Figs S1 and S2; see also Fig. S9 for calibration measurements to convert

The Institute of Scientific and Industrial Research, Osaka University, 8-1 Mihogaoka, Ibaraki, Osaka 567-0047, Japan. Correspondence and requests for materials should be addressed to M.Tsutsui (email: tsutsui@sanken.osaka-u.ac.jp)

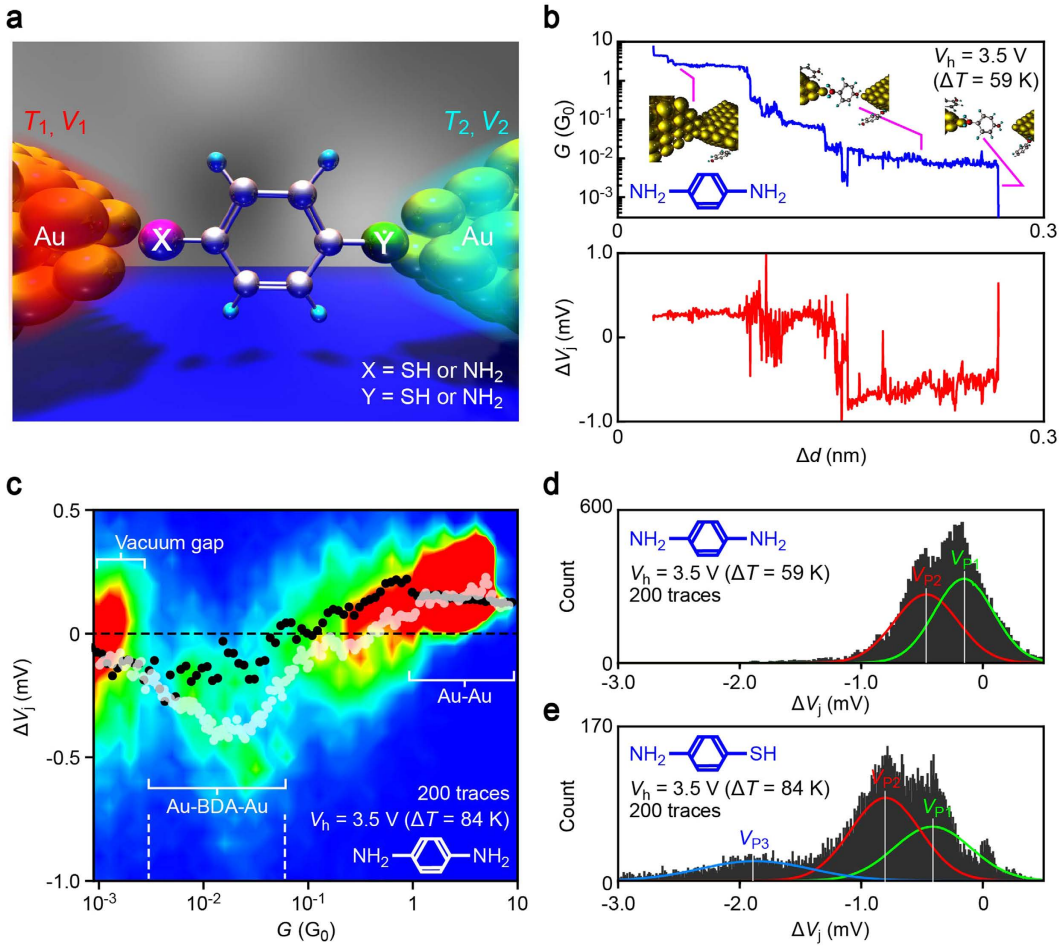

Figure 1. Thermoelectric measurements of molecular junctions. **(a)** Schematic model of single-molecule junctions comprised of a X-benzene-Y molecule bonded to two Au electrodes. Thermopower was measured by imposing a temperature differential through electrical heating of a microheater and probing the thermovoltage. X and Y tested were SH and/or NH_2. **(b)** Conductance (G) and thermovoltage (ΔV_j) traces recorded simultaneously during tensile breakdown of a Au-1,4-benzenediamine-Au bridge under the heater voltage $V_h = 3.5$ V displaying positive and negative thermovoltage of Au nanocontacts and the molecular junction, respectively. **(c)** G versus ΔV_j two-dimensional histogram. White and black plots are the average ΔV_j in cases with and without molecules being added to the junctions, respectively. **(d,e)** ΔV_j distributions constructed with the trace data showing G in a range from 6×10^{-2} G_0 to 0.3×10^{-3} G_0 for benzenediamine (BDA) **(d)** and aminobenzenethiol (ABT) **(e)**. V_{P1}, V_{P2}, and V_{P3} denote the peak positions as defined by Gaussian fit to the histograms represented by solid curves.

V_{piezo} into the junction displacement Δd). The breaking process was implemented for 200 times per V_h condition by reconnecting the Au contact after breakdown of molecular junctions. In each trial, a Au contact was broken at first to create a pair of nanoelectrodes, wherein G decreased to below 1 G_0 in a discrete manner where $G_0 = 2e^2/h$ is the conductance quantum with e and h denoting the electron charge and Planck constant, respectively (Fig. 1b). Thereafter, conductance plateaus were often found at 10^{-2} G_0 to 10^{-3} G_0 suggesting formations of molecular bridges[31]. Meanwhile, the concurrently recorded thermovoltage behaved somewhat synchronously to the change in the conductance (Fig. 1c). Specifically, positive ΔV_j was obtained at $G > 1$ G_α reflecting the negative thermopower $S_{Au} = -\Delta V_j/(\Delta T)$ of Au nanocontacts[32], where ΔT is the temperature difference created therein (see Fig. S8 for estimations of ΔT), owing to the sign of the energy derivative of the density of electronic states at the Fermi level[33]. In contrast, the thermoelectric voltage turns out to be negative at the low conductance regime. The corresponding positive Seebeck coefficient implies charge transport through the highest-occupied molecular orbital (HOMO) levels for the molecules tested[34,35].

Conductance versus thermovoltage characteristics. In order to shed further light on molecular nature in the obtained thermoelectric properties, two-dimensional histograms of G and ΔV_j were constructed (Fig. 1c; see also Fig. S3). The plots conspicuously depict the presence of Au nanocontacts as a cluster of data accumulated at above 1 G_0 with positive ΔV_j. In contrast, the low conductance region below 1×10^{-3} G_0 reveals a regime with negligibly small yet finite thermovoltage on average, which is attributable to tunnelling thermopower

in a vacuum gap[36,37] as corroborated by a control experiment wherein no molecules were added (black plots). On the other hand, there lies another distinct feature at the intermediate range of conductance around 10^{-2} G_0 wherein the negative ΔV_j can be ascribed to the aforementioned HOMO-derived carrier transport in the molecular junctions with relatively large scattering presumably reflecting the geometrical sensitivity of the electronic structure[28,38].

Statistical variations of junction thermopower. Having confirmed the identity of molecular bridges, statistical variations of the thermoelectric voltage was analysed by building ΔV_j histograms with data extracted using a conductance window from 3×10^{-3} G_0 to 6×10^{-2} G_0 whereat the characteristic negative thermoelectric voltage was detected (we note that the single-molecule conductance falls in this range of conductance[39–41]). Interestingly, we found bimodal and trimodal distributions for the symmetric (BDA and BDT) and asymmetric (ABT) molecules, respectively (Fig. 1d; see also Figs S4 and S5). Gaussian fit extracted peaks positioned at V_{P1} through V_{P3}. Plots of V_P, along with the average thermovoltage of Au nanocontacts deduced from ΔV_j at $G > 1$ G_0, with respect to the heater voltage illuminated linear increase in the absolute values of the characteristic thermoelectric voltage with V_h^2 (Fig. 2a–c). This is interpreted as due to the fact that the temperature difference at the junction is produced through the power V_h^2/R_h (R_h is the resistance of the heater) dissipated locally at the Pt micro-coil that heats up one side of the Au leads via thermal conduction through the Al_2O_3 layer[25].

Thermovoltage signatures of molecular junctions. It is of importance to elucidate the origin of the multiple thermovoltage states revealed by the ΔV_j histograms. For this, we inspected the conductance traces of junctions having average thermovoltage $\Delta V_{ave} = \sum(\Delta V_j)/n$ in the low conductance regimes suggestive of molecular bridge formations, where n is the number of data points in each $\Delta V_j - t$ curves (Fig. 2d–g). Interestingly, we found exponential decay in the conductance with respect to the distance d_{gap} between the Au electrodes in case of junctions with $\Delta V_{ave} \geq -0.5$ mV at $V_h = 3.5$ V ($\Delta T = 59$ K), i.e. V_{P1} state, for BDAs (Fig. 2d–e), which is naturally ascribed to electron tunnelling through vacuum gaps instead of charge transport through molecular bridges (Fig. 2f)[42]. In sharp contrast, a plateau was observed at around 8×10^{-3} G_0 for the plots with $\Delta V_{ave} < -0.5$ mV (V_{P2} state) suggesting formations of Au-BDA-Au links (Fig. 2g–i)[40]. Similar trends were seen for the other molecules as well (see Fig. S6). These results imply that whereas V_{P2} is unequivocally attributed to the intrinsic thermoelectric transport characteristics of molecular junctions, V_{P1} is most likely the tunnelling thermopower of a vacuum gap, whose values are in fact close to the low thermovoltage detected for open contacts in the control experiments whereat no molecules are expected between the electrodes. Rough estimation of the barrier height energy Φ from the slope of the conductance decay by assuming $G \propto \exp(-2\kappa d_{gap})$ with the coefficient $\kappa = \sqrt{2m_e\Phi/\hbar^2}$ yields $\Phi = 6.8$ eV with the electron mass $m_e = 9.11 \times 10^{-31}$ kg (Fig. 2d), which is close to the work function of Au[43] thereby corroborating the vacuum tunnelling scenario for V_{P1}.

Stretching-induced thermopower enhancement. The high thermovoltage states of V_{P3} observed for ABT (Fig. 1e) is a superior property from viewpoints of its thermoelectric applications compared to the V_{P2} states. We found that this distinct characteristics arises upon excessive elongation of the molecular junctions (Fig. 3a–d; see also Fig. S7). The stretching effects were also present in BDTs[25,26] but were not evident in the thermovoltage histograms, and thus not considered here in detail due to the relatively short-lived nature of the high-ΔV_j states that emerges on the verge of mechanical breakdown, in comparison to the long lifetime of the Au-thiol linkages. On the other hand, the mechanically-induced thermopower enhancement was confirmed to be completely absent in BDAs indicating important roles of the thiol linkers (Fig. S3d).

Discussion

Direct tunnelling contributions. From a naïve point of view, thermoelectric transport in molecular junctions should accompany an effect of direct tunnelling through vacuum[44]. In order to quantify its possible influence on the measured junction properties, we analysed the conductance versus thermovoltage characteristics in detail. First we noticed that although the positive ΔV_j at $G > 1$ G_0 is suggestive of quantum thermopower of Au nanocontacts (Fig. 1c), a care should be taken on the quantitative interpretation as it is well-established that molecules are often bridging aside the Au atom-sized contacts before the opening of electrode nanogaps[45,46]. This can be seen as multiple batteries, each contributing the single-molecule thermovoltage, with internal resistance R_i connected in parallel when considering no notable quantum interference[47,48] in the thermoelectric transport (Fig. 4a). Then, what we measured was actually the combined voltage described as $\Delta V_j = (V_{Au} m R_{mol} + V_{mol} R_{Au})(R_{mol} R_{Au})/(R_{mol} R_s + R_{Au} R_s + R_{mol} R_{Au})(R_{mol} + R_{Au})$, where $R_{mol} = R_{SMJ}/m$ is the net resistance of m molecules bridging in parallel with the single molecule resistance R_{SMJ}, R_{Au} is the resistance of the Au contacts, and R_s is the serial resistance. This equation tells us that the junction thermovoltage is prone to be determined solely by the source, either molecules or tunnelling gaps, having lower resistance. As R_{SMJ} in the present study is in a range of MΩ[39–41], V_{mol} virtually vanishes and ΔV_j is dominated by that engendered at the Au contacts whereby yielding the positive thermovoltage of the atomic chains at the conductance above 1 G_0. In the meantime, it rapidly decreases to a small negative value as G declines to below 1 G_0, which indicates opening of an electrode gap wherein a few molecules can be connected to the electrodes. Whether molecular feature becomes observable at this stage is thus determined by the relative significance of the thermopower contributions of molecular bridges and vacuum gaps[47]. On the other hand, we find nice fit on the $\Delta V_j - G$ characteristics with the parallel circuit model by assuming four molecules bridging the electrodes ($m = 4$) with $R_{SMJ} = 2.2$ MΩ and $V_{P2} = V_{mol} = 0.47$ mV and variable tunnelling gap size having conductance from 0.1×10^{-3} G_0 to 0.2 G_0 with $V_{gap} = V_{P1} = 0.054$ mV at $V_h = 3.5$ V ($\Delta T = 59$ K) for BDA junctions (Fig. 4b), thus elucidating the non-negligible influence of vacuum tunnelling on the molecular junction thermoelectric transport (Fig. 4c). This in turn suggests the possible use of thermopower for molecular junction diagnosis to assess the vacuum gap contribution as well as to count the number of energy-carrying

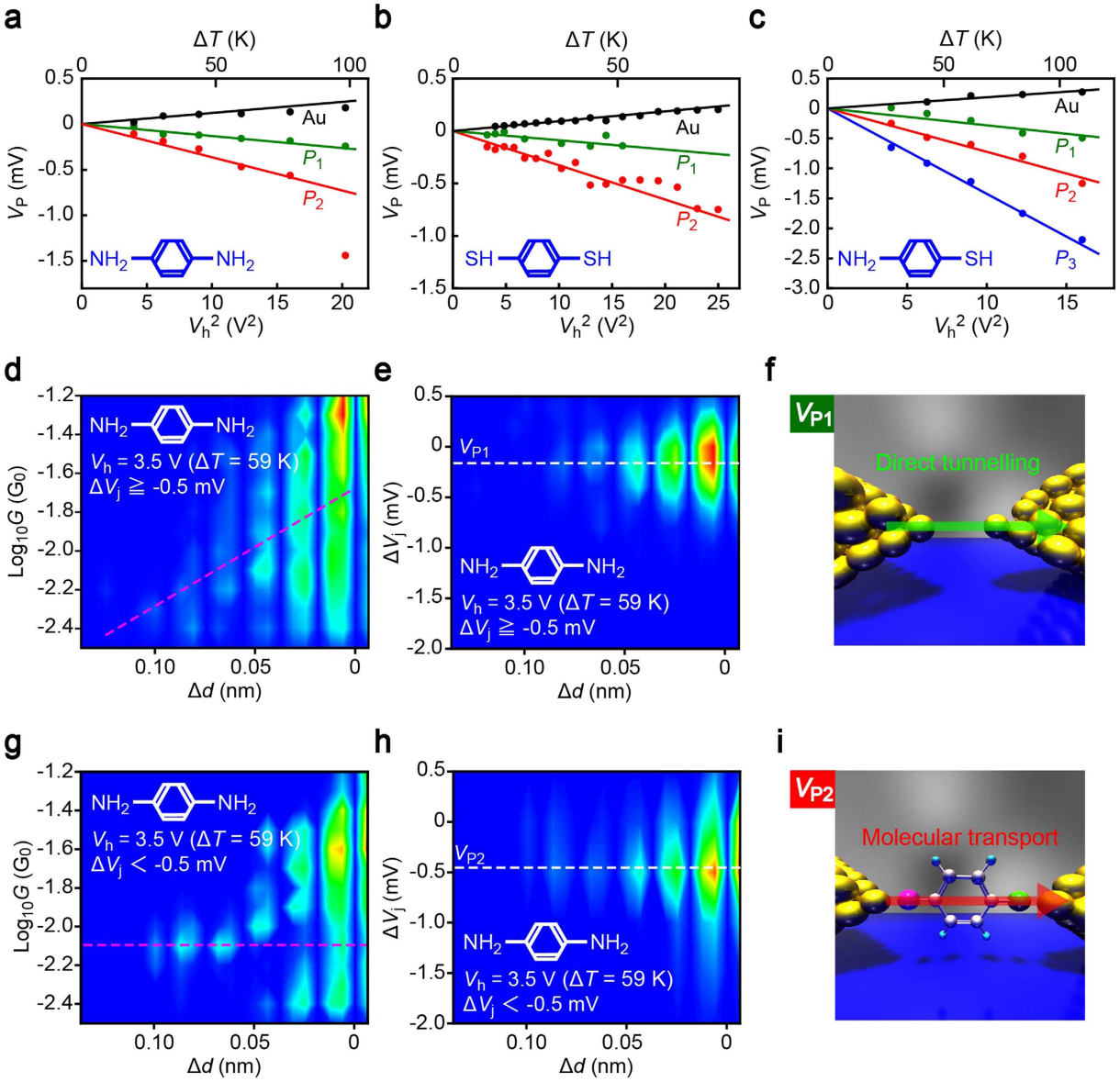

Figure 2. Molecular junction diagnosis. (**a–c**) Characteristic V_P states plotted as a function of V_h^2 and ΔT for BDA (**a**), BDT (**b**), and ABT (**c**). Solid curves are linear fitting to the plots. (**d–f**) Change in G (**d**) and ΔV_j (**e**) under mechanical elongation Δd of Au-BDA-Au junctions showing ΔV_{ave} higher than -0.5 mV at $\Delta T = 59$ K. The exponential decay in G indicates absence of molecules in the electrode gap in case for the thermopower states of V_{P1} (**f**). (**g–i**) High-thermovoltage traces with $\Delta V_{ave} \leq -0.5$ mV (**h**) reveal a plateau at close to the single-molecule conductance (**g**) whereby suggesting electron tunnelling through Au-BDA-Au bridges for V_{P2}. Broken lines in (**d**) and (**g**) show a linear fit to the semi-logarithmic plots and the single-molecule conductance state, respectively.

molecules, which, in the present work, manifested the importance to widen inter-electrode distance to mitigate the detrimental influence of direct tunnelling on the thermoelectric performance of single-molecule junctions.

Anchor dependence of molecular thermopower. Quantitative evaluations of molecular junction thermopower involves intriguing argument about the temperature differential in the atomic scale systems[49]. Here, we instead examined a comparative analysis of the anchor dependence of the molecular junction thermopower by exploiting the Au junctions as an atomic thermometer to characterize the temperature differential. The slope α of the linear $V_{Au} - V_h^2$ dependence constitutes a well-defined Seebeck coefficient of the metal nanocontacts $S_{Au} = -\alpha_{Au}/\beta$ probed in the present measurements, where β is a coefficient that converts the heater voltage to the temperature difference as $\Delta T = \beta V_h^2$. Here, S_{Au} contains a bulk contribution of $S_{bulk} = 1.96\,\mu V/K$[50] in addition to the quantum thermopower S_q at the atom-sized contacts as they were connected to millimeter-long leads. We calculated β by comparing $S_{Au} = S_q - S_{bulk}$ to the experimental $-\alpha_{Au}$ with $S_q = -0.75\,\mu V/K$ for ballistic Au atom-sized contacts[33] whose radius r_c is much smaller than the electron mean free path l in the conductance

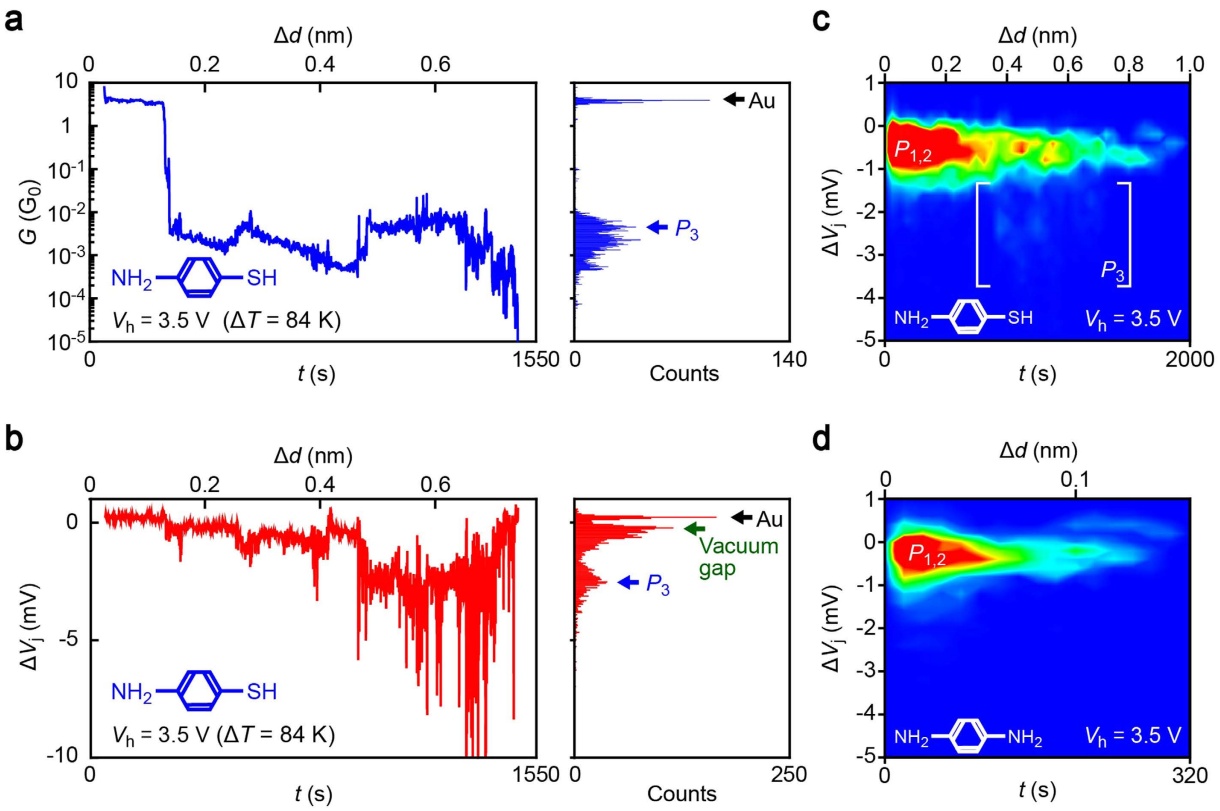

Figure 3. Stretching-induced thermopower enhancement. (**a,b**) G and ΔV_j curves demonstrating increased thermovoltage in a highly-elongated ABT junction. The histograms of the traces reveal the conductance and thermovoltage representative of the junction conditions at each stage of the tensile breakdown. The stretching caused P_3 states with enhanced thermovoltage. (**c,d**) Two-dimensional ΔV_j histograms of ABT (**c**) and BDA junctions (**d**). Note that P_3 states are present only in ABT.

range of $1\ G_0 < G < 5\ G_0$. This yielded $S_{BDT} = 9.5\,\mu V/K$ for V_{P2} of Au-BDT-Au bridges, which fairly agrees with the previous literatures[33]. Comparatively, BDA and ABT exhibited higher thermoelectric power of $S_{ABT} = 10.6\,\mu V/K$ and $S_{BDA} = 10.3\,\mu V/K$, respectively (Fig. 4d).

Geometrical dependence of molecular junction thermopower. We have observed a concomitant enhancement of the conductance and thermopower in highly-stretched thiol-anchored molecular junctions. We explored the underlying contact mechanics by first-principles calculations of junction motifs under various inter-electrode distance conditions L_c, which is defined as the displacement of the molecule-linked Au atoms from the optimized configurations, to unveil the cause of stretching-induced thermopower enhancement observed for the thiolate molecules. We found that while BDAs cannot withstand the tensile straining above 1.6 Å (Fig. 4e), due to the restricted Au-NH_2 bond configurations that hinders the conformational degrees of freedom of molecules in the electrode gap[51], Au-S bond angles and lengths are more amenable to the mechanical stretching reflecting the diverse forms of covalent interactions between the sulphur and Au surface atoms (Fig. 4f)[52], which allowed ABT to take upright conformations. Here, it is worth noting that the Au-S bond in ABT is capable of being elongated by up to 1 Å whereas the NH_2-Au links can be pulled apart by less than 0.3 Å. Under this level of bond elongation, it is anticipated theoretically that G increases by junction stretching due to the entailed shift in the conducting molecular orbital level toward the electrode Fermi level E_F[53–55]. In a framework of single-particle model, the mechanical modulation of molecular states also anticipates thermopower enhancement since the slope of transmission curve at E_F tends to be steeper as the transport becomes closer to a resonance, the overall trend of which explains why the mutual enhancement of G and ΔV_j was observed only in the thiol-anchored molecular junction, thereby suggesting in turn that the electromechanical characteristics would rather be a universal feature in stretched molecular junctions having at least one Au-S link[56], the verification of which calls for future efforts to explore the mechanical effects on various organic molecules other than the mono-benzene derivatives studied in the present work. These findings provide a guide for designing optimal anchoring groups for achieving high thermoelectric power with single-molecule junctions.

Methods

Fabrication of heater-embedded MCBJs. Microelectrodes were formed on a polyimide coated phosphor bronze substrate by photolithography and radio-frequency magnetron sputtering of a Cr/Au (2 nm/50 nm thickness) layer followed by lift-off through sonication in *N,N*-dimethylformamide. Subsequently, Al_2O_3 thermal

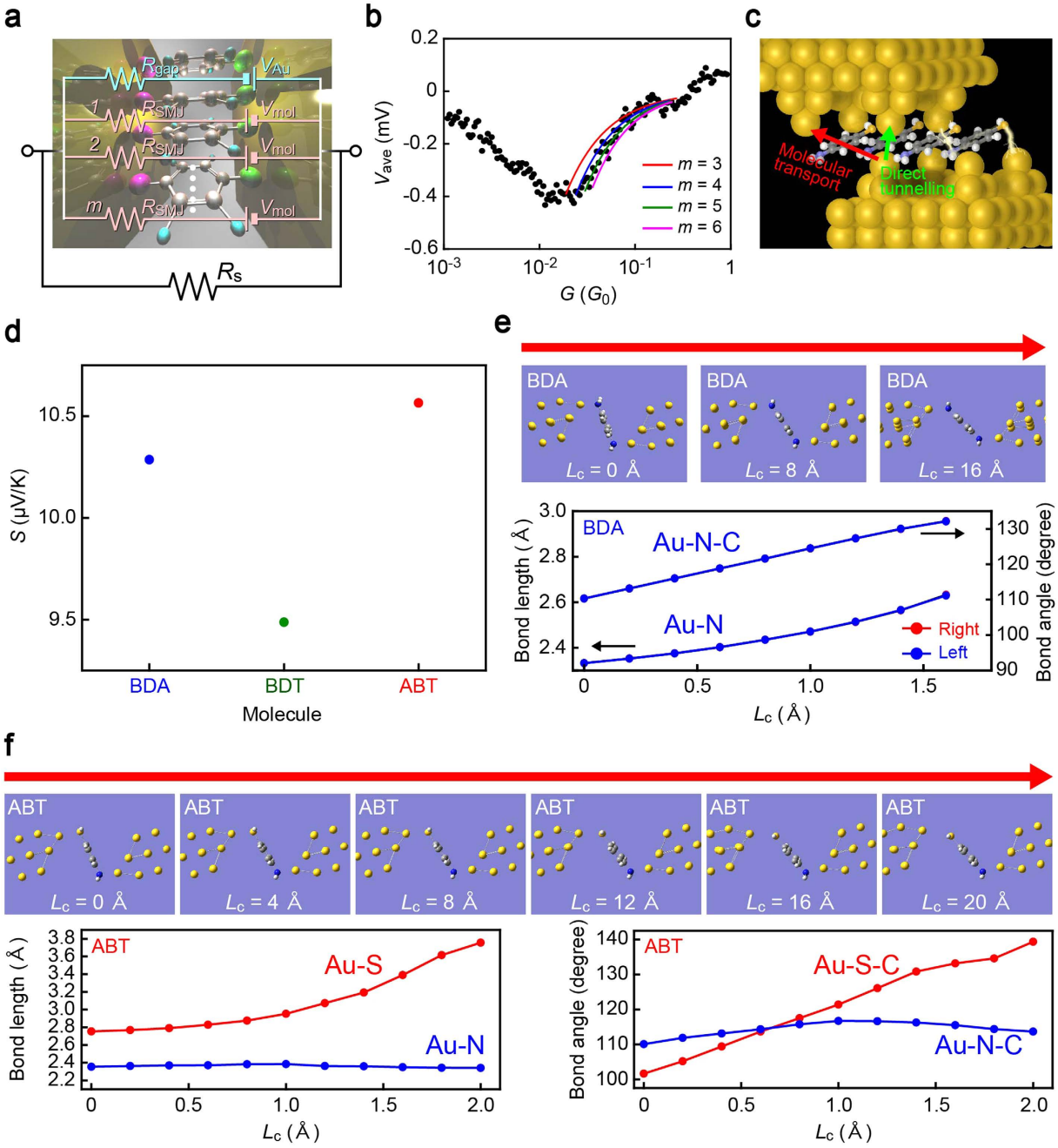

Figure 4. Anchor-dependent contact mechanics. (**a**) Equivalent circuit of molecular junctions consisting of m molecules with resistance R_{SMJ} and thermovoltage V_2 bridging a Au electrode gap. Contribution of direct tunnelling is included as the resistance R_{gap} and the tunnelling thermopower component V_{gap} connected in parallel. R_s is the thermovoltage sensing resistor connected in series to the junctions. (**b**) Direct tunnelling contribution. The thermovoltage versus conductance characteristics complies with the circuit model assuming quadruple-molecule junctions with variable size of vacuum gap with $1/R_{gap}$ from 1×10^{-4} G_0 to 1×10^{-1} G_0. (**c**) Energy-optimized structure of BDA quadruple-molecule junctions. (**d**) Seebeck coefficients S estimated by taking the thermopower of Au nanocontacts as reference. (**e,f**) Contact mechanics of BDA (**e**) and ABT (**f**). Junction images show energy-optimized structures. Arrows point toward stretching of junctions defined as the distance L_c between the molecule-linked Au atoms. Au-molecule bond lengths and angles at the both sides are plotted with respect to L_c.

bath was created by electron beam lithography, inductively-coupled plasma sputter deposition of Al_2O_3 (40 nm thick), and the lift-off process. On the heat reservoir, Pt coils and a Au nanojunction were further prepared by two additional electron beam lithography processes. Finally, the polyimide layer was deep-etched by 2 μm in depth through reactive ion etching using O_2 etchant gas so as to free the Au junction from the substrate. The

free-standing length of the junction was approximately 2 μm, which provided the attenuation factor r of 1.3×10^{-4} as calibrated by measuring electrode gap size dependence of the tunnelling current (Fig. S9).

Formations of molecular junctions. A heater-embedded MCBJ was mounted on a sample stage where there were two counter supports. On the other side, there was a piezo-driven pushing rod that expands or shrink by changing the voltage V_p by ΔV_p with ratio $-1\,\mu m/V_p$. In experiments, a droplet of dilute toluene solution of molecules (either BDA, BDT, or ABT) at concentration 5 μM was added on a Au junction. The MCBJ beam was then bent mechanically by moving the pushing rod to break the Au junction, which led to the molecules to adhere chemically on the fracture surface. A chamber was then evacuated to a pressure around 10^{-6} Torr so as to remove the solvent. Thereafter, stretching of the junction was implemented by a feedback control of the piezo-actuator expansion. Specifically, the strain rate was set to 1 nm/s during elongation of Au nanocontacts until G decreased to below 6 G_0. After that, the junction elongation speed was set to be 0.5 pm/s by applying a V_p ramp of 4 mV/s. This slow straining yielded enough amount of time for precise measurements of the junction thermopower and conductance. When G eventually dropped to lower than 10^{-5} G_0, Au electrodes were reconnected. The series of breaking/connecting processes were repeated for 200 times at each V_h condition from 2.0 V to 5.0 V.

Thermoelectric voltage and electrical conductance measurements. The electrical conductance and thermovoltage of junctions were measured simultaneously during the tensile stretching. For this, a constant dc bias voltage V_h was applied to a Pt microheater throughout the experiments to create a temperature differential at the junctions necessary to induce detectable amount off thermovoltage. Furthermore, a picoammeter/source unit (Keithley 6487) was used to apply the dc voltage $V_b = 0.1$ V and acquire the current flowed through the junctions, from which the conductance $G = I/V_b$ was obtained (the deduction included subtraction of a serial resistance). After the acquisition of G, V_b was set to zero and the potential drop V_m at the thermovoltage-sensing resistor having variable resistance R_s from 10 kΩ to 1 MΩ was obtained using a nanovoltmeter (Keithley 2182). R_s was changed electrically during the junction breaking in response to G by using a home-built relay device. The junction thermoelectric voltage ΔV_j was computed from V_m considering the division at R_s and $1/G$. Subsequently, V_b was switched back to 0.1 V for the next conductance measurement. The sampling rate of G and V_m was about 3 Hz.

First-principle calculations. Gaussian 09 package was employed to characterize mechanical stretching effects on molecular junction configurations. The atomic motifs of a single-molecule junction were modelled by respectively placing BDA, or ABT between two Au14 clusters. Density functional theory (DFT) level of calculations were performed with B3LYP hybrid functional for optimizing the junction structures. The basis sets of 6–31 G + (d, p) and LANL2DZ were employed for (C, H, S, N) and (Au), respectively. Completing the optimization processes, the distance between the two molecule-linking Au atoms was widened gradually by 0.2 Å steps. At every each step, the structural optimization was performed and the bond length as well as the angle at the metal-molecule links were measured from the coordination of the atoms. The series of calculations were continued until the molecules bridged the Au clusters.

Theoretical derivation of quadruple molecular junction strucutre. To deduce the parallel bridging structure of multiple molecules in an electrode gap, we started modelling from an optimized structure of a single-molecule junction wherein ABT is placed between two Au14 clusters. In the optimized geometry, N-C and S-C bonds of the ABT molecule leaned to 97.4° and 99.7° from [111] direction of each Au14 cluster. By expanding a Au14-ABT-Au14 motif to Au22-ABT-Au22 structure, we constructed the slab model of 3×3 supercell and then conducted geometry and cell optimization calculations by using a density functional based tight binding (DFTB) method with the AuOrg Slater-Koster parameters under a periodic boundary condition. All calculations were performed by using Material Studio package. The optimized lattice parameters were $a = b = 8.02$ Å and $c = 42.9$ Å, $\alpha = 118°$, $\beta = 117°$ and $\gamma = 61.0°$, and the atomic distance of Au for molecular transport and direct tunnelling was evaluated as 9.52 Å and 6.29 Å, respectively[55,56].

References

1. Priya, S. & Inman, D. J. *Energy harvesting technologies*. (Springer, 2009).
2. Zebarjadi, M., Esfarjani, K., Dresselhaus, M. S., Ren, Z. F. & Chen, G. Perspectives on thermoelectrics: from fundamentals to device applications. *Energy Environ. Sci.* **5,** 5147–5162 (2012).
3. Elsheikh, M. H. *et al.* A review on thermoelectric renewable energy: Principle parameters that affect their performance. *Renew. Sustain. Energy Rev.* **30,** 337–355 (2014).
4. Goldsmid, H. J. *Review of thermoelectric materials*. Vol. 121, 153–195 (Springer, 2016).
5. Sootsman, J. R., Chung, D. Y. & Kanatzidis, M. New and old concepts in thermoelectric materials. *Angew. Chem. Int. Ed.* **48,** 8616–8639 (2009).
6. Hicks, L. D. & Dresselhaus, M. S. Thermoelectric figure of merit of a one-dimensional conductor. *Phys. Rev. B* **47,** 16631 (2007).
7. Heremans, J. P., Dresselhaus, M. S., Bell, L. E. & Morelli, D. T. When thermoelectrics reached the nanoscale. *Nat. Nanotechnol.* **8,** 471–473 (2013).
8. Vineis, C. J., Shakouri, A., Majumdar, A. & Kanatzidis, M. G. Nanostructured thermoelectrics: big efficiency gains from small features. A*dv. Mater.* **22,** 3970–3980 (2010).
9. Li, J.–F., Liu, W.–S., Zhao, L.–D. & Zhou, M. High-performance nanostructured thermoelectric materials. *NPG Asia Mater.* **2,** 152–158 (2010).
10. Chen, Z.–G., Han, G., Yang, L., Cheng, L. & Zou, J. Nanostructured thermoelectric materials: current research and future challenge. *Prog. Nat. Sci.* **22,** 535–549 (2012).
11. Martin-Gonzalez, M., Caballero-Calero, O. & Diaz-Chao, P. Nanoengineering thermoelectric for 21st century: energy harvesting and other trends in the field. *Renew. Sustain. Energy Rev.* **24,** 288–305 (2013).
12. Harman, T. C., Taylor, P. J., Walsh, M. P. & LaForge, B. E. Quantum dot superlattice thermoelectric materials and devices. *Science* **297,** 2229–2232 (2002).
13. Hochbaum, A. I. *et al.* Enhanced thermoelectric performance of rough silicon nanowires. *Nature* **451,** 163–168 (2007).

14. Mahan, G. D. & Sofo, J. O. The best thermoelectric. *Proc. Natl. Acad. Sci. USA* **93,** 7436–7439 (1996).
15. Dubi, Y. & Di Ventra, M. Colloquium: Heat flow and thermoelectricity in atomic and molecular junctions. *Rev. Mod. Phys.* **83,** 131–155 (2011).
16. Malen, J. A., Yee, S. K., Majumdar, A. & Segalman, R. A. Fundamentals of energy transport, energy conversion, and thermal properties in organic-inorganic heterojunctions. *Chem. Phys. Lett.* **491,** 109–122 (2010).
17. Rincon-Garcia, L., Evangeli, C., Rubio-Bollinger, G. & Agrait, N. Thermopower measurements in molecular junctions. *Chem. Soc. Rev.* **45,** 4285–4306 (2016).
18. Zimbovskaya, N. A. Seebeck effect in molecular junctions. *J. Phys.: Condens. Matter* **28,** 183002 (2016).
19. Malen, J. A. *et al.* Identifying the length dependence of orbital alignment and contact coupling in molecular heterojunctions. *Nano Lett.* **9,** 1164–1169 (2009).
20. Widawsky, J. R. *et al.* Length-dependent thermopower of highly-conducting Au-C bonded single molecule junctions. *Nano Lett.* **13,** 2889–2894 (2013).
21. Dell, E. J., Capozzi, B., Xia, J., Venkataraman, L. & Campos, L. M. Molecular length dictates the nature of charge carrier in single-molecule junctions of oxidized oligothiophenes. *Nat. Chem.* **7,** 209–214 (2015).
22. Evangeli, C. *et al.* Engineering the thermopower of C_{60} molecular junctions. *Nano Lett.* **13,** 2141–3245 (2013).
23. Kim, Y., Jeong, W., Kim, K., Lee, W. & Reddy, P. Electrostatic control of thermoelectricity in molecular junctions. *Nat. Nanotechnol.* **9,** 881–885 (2014).
24. Rincon-Garcia, L. *et al.* Molecular design and control of fullerene-based bi-thermoelectric materials. *Nat. Mat.* **15,** 289–294 (2016).
25. Tsutsui, M., Morikawa, T., He, Y., Arima, A. & Taniguchi, M. High thermopower of mechanically stretched single-molecule junctions. *Sci. Rep.* **5,** 11519 (2015).
26. Torres, A., Pontes, R. B., da Silva, A. J. R. & Fazzio, A. Tuning the thermoelectric properties of a single-molecule junction by mechanical stretching. *Phys. Chem. Chem. Phys.* **17,** 5386 (2015).
27. Dubi, Y. Possible origin of thermoelectric response fluctuations in single-molecule junctions. *New J. Phys.* **15,** 105004 (2013).
28. Basch, H. & Ratner, M. A. Interface geometry and molecular junction conductance: geometric fluctuation and stochastic switching. *Nano Lett.* **5,** 1668–1675 (2005).
29. Burkle, M., Hellmuth, T. J., Pauly, F. & Asai, Y. First-principles calculation of the thermoelectric figure of merit for [2,2] paracyclophane-based single-molecule junctions. *Phys. Rev. B* **91,** 165419 (2015).
30. Manrique, D. Z., Al-Galiby, Q., Hong, W. & Lambert, C. J. A new approach to materials discovery for electronic and thermoelectric properties of single-molecule junctions. *Nano Lett.* **16,** 1308–1316 (2016).
31. Xu, B. & Tao, N. J. Measurement of single-molecule resistance by repeated formation of molecular junctions. *Science* **301,** 1221–1223 (2003).
32. Tsutsui, M., Morikawa, T., Arima, A. & Taniguchi, M. Thermoelectricity in atom-sized junctions at room temperatures. *Sci. Rep*. **3,** 3326 (2013).
33. Evangeli, C. *et al.* Quantum thermopower of metallic atomic-size contacts at room temperature. *Nano Lett.* **15,** 1006–1011 (2015).
34. Reddy, P., Jang, S.–Y., Segalman, R. A. & Majumdar, A. Thermoelectricity in molecular junctions. *Science* **315,** 1568–1571 (2007).
35. Quek, S. Y., Choi, H. J., Louie, S. G. & Neaton, J. B. Thermopower of amine-gold linked aromatic molecular junctions from first principles. *ACS Nano* **5,** 551–557 (2011).
36. Marschall, J. & Majumdar, A. Charge and energy transport by tunnelling thermoelectric effect. *J. Appl. Phys.* **74,** 4000 (1993).
37. Maksymovych, P., Kelly, S. J. & Cerda, J. I. Surface-state enhancement of tunnelling thermopower on the Ag(111) surface. *ACS Nano* **8,** 12110–12119 (2014).
38. Adak, O. *et al.* Flicker noise as a probe of electronic interaction at metal-single molecule interfaces. *Nano Lett.* **15,** 4143–4149 (2015).
39. Tsutsui, M., Taniguchi, M. & Kawai, T. Quantitative evaluation of metal-molecule contact stability at the single-molecule level. *J. Am. Chem. Soc.* **131,** 10552–10556 (2009).
40. Venkataraman, L. *et al.* Single-molecule circuits with well-defined molecular conductance. *Nano Lett.* **6,** 458–462 (2006).
41. Xiao, X., Xu, B. & Tao, N. J. Measurement of single molecule conductance: benzenedithiol and benzenedimethanethiol. *Nano Lett.* **4,** 267–271 (2004).
42. Yee, S. K., Malen, J. A., Majumdar, A. & Segalman, R. A. Thermoelectricity in fullerene-metal heterojunctions. *Nano Lett.* **11,** 4089–4094 (2011).
43. Michaelson, H. B. The work function of the elements and its periodicity. *J. Appl. Phys.* **48,** 4729 (1977).
44. Quan, R., Pitler, C. S., Ratner, M. A. & Reuter, M. G. Quantitative interpretations of break junction conductance histograms in molecular electron transport. *ACS Nano* **9,** 7704–7713 (2015).
45. Huisman, E. H. *et al.* Stabilizing single-atom contacts by molecular bridge formation. *Nano Lett.* **8,** 3381–3385 (2008).
46. Tsutsui, M., Taniguchi, M. & Kawai, T. Atomistic mechanics and formation mechanism of metal-molecule-metal junctions. *Nano Lett.* **9,** 2433–2439 (2009).
47. Vazquez, H. *et al.* Probing the conductance superposition law in single-molecule circuits with parallel paths. *Nat. Nanotechnol.* **7,** 663–667 (2012).
48. Lambert, C. J. Basic concepts of quantum interference and electron transport in single-molecule electronics. *Chem. Soc. Rev.* **44,** 875–888 (2015).
49. Dubi, Y. & Di Ventra, M. Thermoelectric effects in nanoscale junctions. *Nano Lett.* **9,** 97–101 (2009).
50. Blatt, F. J. *Thermoelectric power of metals.* (Plenum Press, 1976).
51. Quek, S. Y. *et al.* Amine-gold linked single-molecule circuits: experiment and theory. *Nano Lett.* **7,** 3477–3482 (2007).
52. Tachibana, M., Yoshizawa, K., Ogawa, A., Fujimoto, H. & Hoffmann, R. Sulfur-gold orbital interactions which determine the structure of alkanethiolate/Au(111) self-assembled monolayer systems. *J. Phys. Chem. B* **106,** 12727–12736 (2002).
53. Bruot, C., Hihath, J. & Tao, N. Mechanically controlled molecular orbital alignment in single molecule junctions. *Nat. Nanotechnol.* **7,** 35–40 (2012).
54. Andrews, D. Q., Cohen, R., van Duyne, R. P. & Ratner, M. A. Single molecule electron transport junctions: charging and geometric effects on conductance. *J. Chem. Phys.* **125,** 174718 (2006).
55. Pontes, R. B., Rocha, A. R., Sanvito, S., Fazzio, A. & da Silva, A. J. R. *Ab initio* calculations of structural evolution and conductance of benzene-1,4-dithiol on gold leads. *ACS Nano* **5,** 795–804 (2011).
56. Saffarzadeh, A., Demir, F. & Kirczenow, G. Mechanism of the enhanced conductance of a molecular junction under tensile stress. *Phys. Rev. B* **89,** 045431 (2014).

Acknowledgements

This research was supported in part by the Japan Society for the Promotion of Science (JSPS) KAKENHI Grant Number 15H03543 and "Nanotechnology Platform Project (Nanotechnology Open Facilities in Osaka University)" of Ministry of Education, Culture, Sports, Science and Technology, Japan [No: F-12-OS-0016]. M. Tsutsui acknowledges support from Foundation Advanced Technology Institute, Kansai Research Foundation for technology promotion, Yazaki Memorial Foundation for Science and Technology, and The Asahi Glass Foundation.

Author Contributions

M. Tsutsui planned and designed experiments. M.T. and T.M. fabricated microheater-embedded MCBJs and conducted break junction measurements. M.T., T.M., K.Y., and M.T. performed data analyses. K.Y. carried out first-principle calculations. M. Tsutsui wrote paper.

Additional Information

Supplementary information accompanies this paper at http://www.nature.com/srep

Competing Interests: The authors declare no competing financial interests.

How to cite this article: Tsutsui, M. *et al.* Roles of vacuum tunnelling and contact mechanics in single-molecule thermopower. *Sci. Rep.* **7**, 44276; doi: 10.1038/srep44276 (2017).

Publisher's note: Springer Nature remains neutral with regard to jurisdictional claims in published maps and institutional affiliations.